Robotic endoscopic system for fine needle aspiration of liver lesions

Raghav Khanna[1,2] Nikola Fischer[1] Zhenting Du[1] Christos Bergeles[1]

1. School of Biomedical Engineering and Imaging Sciences, King's College London
2. Guy's, King's and St. Thomas' School of Medicine

Background

Liver lesions are currently aspirated/biopsied through percutaneous, laparoscopic or endoscopic approaches[1]. The latter procedure, endoscopic ultrasound guided fine needle aspiration (EUS-FNA), typically uses a straight, rigid 19G needle inserted through the stomach into the liver[1]. This method has key limitations, including limited reachability to lesions in the right lobe of the liver and a steep learning curve[2]. To address this, we propose the design of a tendon driven endoscope and steerable needle with a deep learning algorithm for automated path planning.

Methods

First stage continuum endoscope:

This four degree of freedom (DoF) tendon driven robot consists of two segments composed of modular spacer discs arranged in series. The discs have a central channel for a spring backbone, six (proximal segment) or three (distal segment) peripheral channels for routing steel wire tendons and a male-female mating surface that form constrained revolute joints with each other.

The robot is actuated by six servos fixed in place by a lower and upper plate (Fig. 1). These servos rotate pulleys that create tendon tension. Servos are arranged in pairs, offset by 3 mm in height. The middle pair is offset by 2 mm laterally. This arrangement accommodates the symmetrical antagonistic pairing of the tendons.

Inverse kinematics is calculated using FABRIKc, a constant curvature solver for multi-segment continuum robots that creates virtual links and iteratively adjusts bending angles and orientations to match the tip to a desired pose[3].

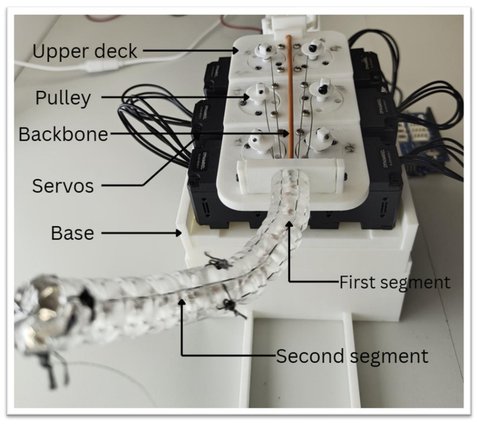

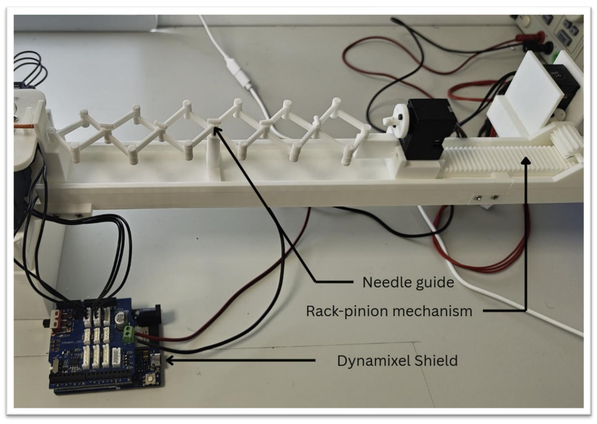

(Left) Figure 1. Continuum endoscope
(Right) Figure 2. steerable needle

Second stage steerable needle:

This stage actuates the super-elastic Nickel-Titanium needle through the gelatin liver phantom. The needle naturally bends within tissue due to the asymmetric forces exerted on the angled bevel tip. Two DoF control (translation and rotation) allow for straight motion, bending motion and changes to the bending plane. The main limitation is the small curvature; this was addressed by creating deep notches for increased local curvature. An accordion style needle guide was constructed to prevent needle kinking as it was advanced through tissue (Fig. 2).

For trajectory planning, an online, off-policy soft actor critic deep reinforcement learning algorithm with clipped double Q and a maximum entropy approach was designed. The reward policy used rewards distance reduction, straight motion, entering a target region, hitting the target (within 3 mm) and the early conclusion of an episode. Hitting an obstacle results in a large penalty and episode termination. Training uses a 200k replay buffer (batch 256) with one update per step.

Figure 3. A – first stage tests with magnetic NDI system
B – needle moving through phantom.
C – Camera based needle tip tracking

Conclusion

Results demonstrate the basic technical feasibility of a flexible system for EUS-FNA, with increased reachability of deep-seated lesions in the liver. This design can be extended to aspiration, biopsy and ablation in other GI structures.

Results

Evaluation	n	Euclidean MAE (mm)	Euclidean RMSE (mm)	Euclidean SD (mm)
Position only FABRIKc	75 points	20.86	22.17	7.58
Position and orientation	75 points	20.44	21.84	7.80
Repeatability	32 points	-	-	0.27
NeedleNav	32 trajectories	18.83	19.98	6.91

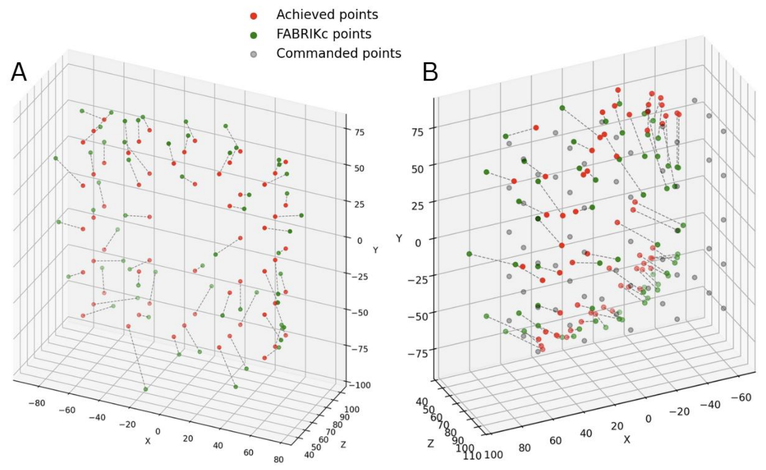

Figure 4. A – commanded versus achieved points, position only control.
B – position and orientation control. Euclidean errors are in the table above.

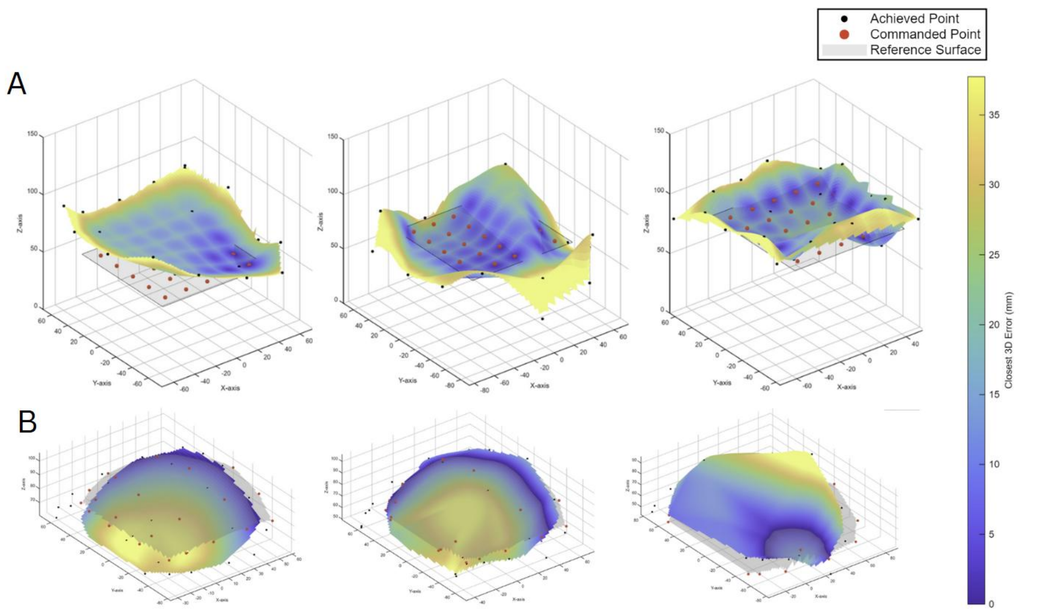

Figure 5. Heat maps demonstrating 3D Euclidean error for the endoscope. A – position only testing, B – position and orientation testing. Bivariate cubic interpolation was used to generate surfaces for the commanded points and achieved points.

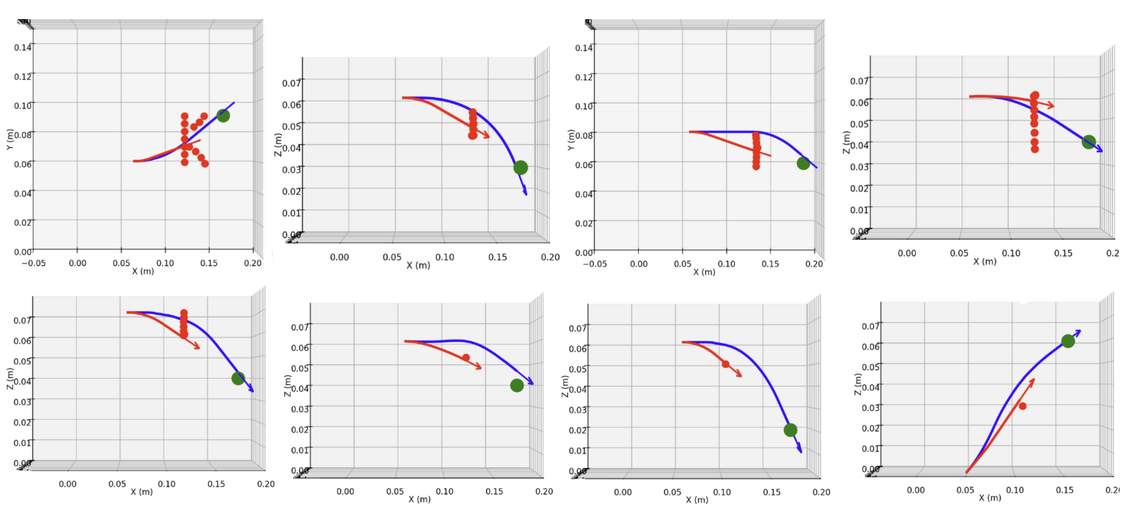

Figure 6. Needle trajectories, **red** representing models trained without obstacle avoidance, and **blue** with obstacles (**red circles**) for the same target (**green**).

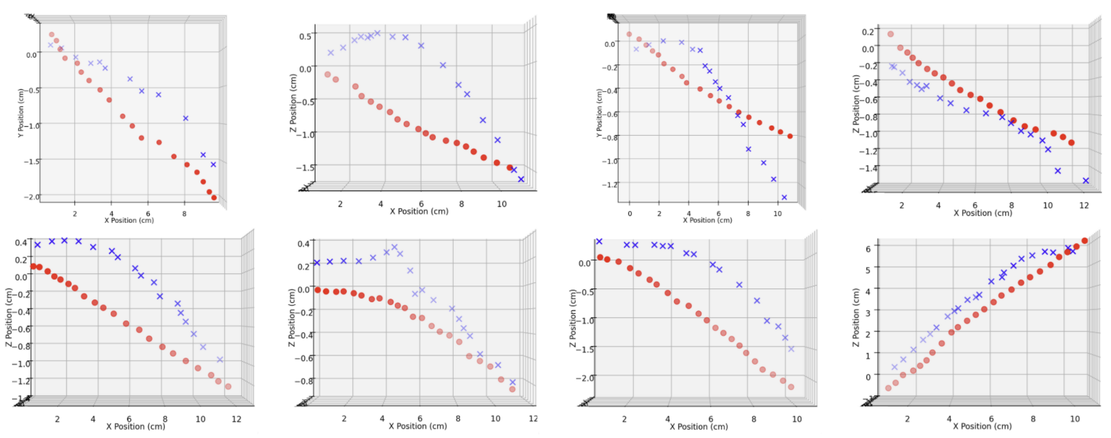

Figure 7. Real obstacle trajectories in **blue** and non-obstacle trajectories in **red**.

References: 1) Neuberger, J. *et al.* (2020) 'Guidelines on the use of liver biopsy in clinical practice from the British Society of Gastroenterology, the Royal College of Radiologists and the Royal College of Pathology', *Gut*, 69(8), pp. 1382–1403. doi:10.1136/gutjnl-2020-321299.
2) ICHIM, V.A. *et al.* (2022) 'Endoscopic ultrasound-guided biopsy of liver tumors', *In Vivo*, 36(2), pp. 890–897. doi:10.21873/invivo.12778.
3) Kolpashchikov, D.Y. *et al.* (2018) 'FABRIK-Based Inverse Kinematics For Multi-Section Continuum Robots', *2018 18th International Conference on Mechatronics - Mechatronika (ME)*, pp. 1–8.